

# A CMP-based [FeFe]-hydrogenase dual-functional biomimetic system for photocatalytic hydrogen evolution coupled with degradation of tetracycline

Guangyuan Feng<sup>a</sup>, Yajing Sun<sup>a</sup>, Jiangyan Yuan<sup>a</sup>, Jingyu Qian<sup>d</sup>, Nasreldeen Siam<sup>a</sup>, Dejuan Fa<sup>a</sup>, Wenyan Ji<sup>a</sup>, Enbing Zhang<sup>a</sup>, Yongtao Shen<sup>a</sup>, Jing Yan<sup>a,\*</sup>, Shengbin Lei<sup>a,\*</sup>, Wenping Hu<sup>a,b,c,\*\*</sup>

<sup>a</sup> Tianjin Key Laboratory of Molecular Optoelectronic Sciences, Department of Chemistry, School of Science, Tianjin University & Collaborative Innovation Center of Chemical Science and Engineering, Tianjin 300072, China

<sup>b</sup> Beijing National Laboratory for Molecular Science, Key Laboratory of Organic Solids, Institution of Chemistry, Chinese Academy of Sciences, Beijing 100190, China

<sup>c</sup> Joint School of National University of Singapore and Tianjin University, Fuzhou International Campus, Tianjin University, Binhai New City, Fuzhou 350207, China

<sup>d</sup> Changzhou Zhuojun Technology Co., Ltd, China

## ARTICLE INFO

### Keywords:

Biomimetic catalyst  
Conjugated microporous polymer  
[FeFe]-Hydrogenase  
Photocatalytic Hydrogen Evolution  
Tetracycline degradation

## ABSTRACT

A novel bio-inspired conjugated microporous polymer (CMP) had been designed, synthesized and characterized. The mimics of [FeFe]-hydrogenase active sites were covalently attached to the CMP skeleton, which facilitates charge transfer between the light-harvesting moiety and active sites, and exhibited high performance in visible-light photocatalytic hydrogen evolution ( $2120 \mu\text{mol}\cdot\text{h}^{-1}\cdot\text{g}^{-1}$ ) in an aqueous solution. The flower-like morphology, covalently linked framework and the “single active-site” effect derived from the porous skeleton were deemed to go a long way toward boosting the properties above. Interestingly, when the electron sacrifice agent (triethanolamine) was replaced by tetracycline, the CMP-based photocatalyst maintained the capability of photocatalytic hydrogen production ( $370 \mu\text{mol}\cdot\text{h}^{-1}\cdot\text{g}^{-1}$ ) and realized efficient photodegradation of tetracycline simultaneously. This work provides a heuristic green dual-function strategy for constructing a sustainable and efficient photocatalytic system for hydrogen evolution with concurrent antibiotic residue degradation.

## 1. Introduction

Photocatalytic hydrogen ( $\text{H}_2$ ) evolution driven by solar energy has received increasing research interest owing to its efficient solar-to-chemical conversion, providing a potentially clean and sustainable solution to the related environmental issues [1]. One of the toughest challenges that remain in solar-driven  $\text{H}_2$  evolution is to enhance the activity of the photocatalytic systems while minimizing the consumption of expensive (and possibly toxic) electron sacrifices and co-catalysts [2,3]. As known, some nature-inspired biomimetic systems without costly and toxic composition are reasonably regarded as a competitive alternative to guide the way to a green and sustainable solution [4]. Conjugated microporous polymers (CMP) or covalent organic frameworks (COFs) have been emerged as new materials in this context, which have structural and chemical tunability, high specific surface area and porosity, extended  $\pi$ -conjugation and excellent optoelectronic properties [5]. Recently, some COF-based photocatalysts have been

successfully applied to photocatalytic hydrogen evolution reaction (HER). In these studies, precious metal platinum (Pt) was used as the most popular co-catalyst for the photocatalytic system [6], while some earth-abundant metal (Ni or Co) related molecular co-catalysts also achieve encouraging effects [7,8]. Thereinto, chloro(pyridine)cobaloxime and related complexes have been physisorbed [9] or postsynthetic [10] tethered to COFs, which show improved and prolonged photocatalytic activity with respect to molecular catalysts. As another alternative for noble-metal catalysts, [FeFe]-hydrogenase models, inspired by the structure of active site of natural [FeFe]-hydrogenase (Fig. 1a) [11] which can catalyze  $\text{H}_2$  production with a turnover frequency (TOF) of  $6000\text{--}9000 \text{s}^{-1}$  [12], had been studied in various artificial photocatalytic hydrogen evolution systems [13]. Herein, in order to improve the reactivity and durability of the H-cluster mimics, we designed and synthesized a bio-inspired photocatalyst (TAPP-[2Fe2S]-CMP), in which the [2Fe2S]-cluster was covalently linked to the dialdehyde building block and thus covalently linked to the resulting CMP architecture

\* Corresponding authors.

\*\* Corresponding author at: Tianjin Key Laboratory of Molecular Optoelectronic Sciences, Department of Chemistry, School of Science, Tianjin University & Collaborative Innovation Center of Chemical Science and Engineering, Tianjin 300072, China.

E-mail addresses: [jingyan@tju.edu.cn](mailto:jingyan@tju.edu.cn) (J. Yan), [shengbin.lei@tju.edu.cn](mailto:shengbin.lei@tju.edu.cn) (S. Lei), [huwp@tju.edu.cn](mailto:huwp@tju.edu.cn) (W. Hu).

(Fig. 1b). The covalent linkage both benefits the well spatial arrangement of active sites and facilitates the charge transfer between light-harvesting porphyrin moiety and active [2Fe2S] sites, thus our catalyst exhibited good stability and optimal efficiency [14–16].

For economic and environmental concerns, the over-dependence on electronic sacrificial reagents has been one of the limiting factors hindering the industrial application of photocatalytic systems [17]. To address this problem, the electron sacrifice agent (triethanolamine, TEOA) was replaced by a clinical broad-spectrum naphthalene antibiotic, tetracycline (TC). In this way, we constructed a new CMP-based bionic dual-functional system, which couples the H<sub>2</sub> generation and antibiotic residue removal processes together in aqueous solution [18, 19]. Our exploration of CMP-based [FeFe]-hydrogenase biomimetic system may pave the way for constructing highly stable photocatalytic systems with high solar-to-hydrogen efficiencies while abating the pollution to the living ecosystems and consumption of scarce resources as far as possible.

## 2. Experimental section

### 2.1. Preparation of TAPP-[2Fe2S]-CMP

The TAPP-[2Fe2S]-CMP were carried out by a Schiff-base condensation reaction. In a typical procedure, the mixture of 5,10,15,20-tetraakis(4-aminophenyl)porphyrin (TAPP) (13 mg, 0.02 mmol) and 2 (48 mg, 0.04 mmol), and a mixed solvent of chloroform/acetic acid (4:0.2 mL) was successively added into a 10 mL Pyrex tube. The mixture was then sonicated for 20 min. The Pyrex tube was degassed through three freeze-pump-thaw cycles. The tube was flame-sealed and kept static for 72 h at 30 °C. The precipitate was collected by centrifugation, washed with tetrahydrofuran (THF) and acetone, and then dried under vacuum at room temperature for 12 h to achieve the TAPP-[2Fe2S]-CMP. We have tried different reaction conditions including different solvents and hybrid solvents, different temperatures and catalysts, which were summarized in Table S3. However, the samples obtained from the attempts above were all amorphous.

## 2.2. Photocatalytic experiments

### 2.2.1. Photocatalytic hydrogen evolution

The photocatalyst (2.5 mg) was dispersed in an aqueous solution (5 mL) containing triethanolamine (TEOA) (50 µL), which was saturated with nitrogen gas and sealed with an airtight cap. A photocatalytic reactor (400 W metal halide lamp) with a cutoff filter ( $\lambda > 380$  nm) was used as the light source. The produced photoproduct of H<sub>2</sub> was characterized by gas chromatography (GC) analysis with a thermal conductivity detector (TCD) using nitrogen as the carrier gas. The system kept on swirling by a magneton during the photocatalytic process. The control experiments followed the same procedure as mentioned above without TAPP-[2Fe2S]-CMP, irradiation or TEOA. In order to evaluate recyclability and stability of TAPP-[2Fe2S]-CMP, the photocatalyst was centrifuged and washed with water after photocatalytic hydrogen evolution reaction and then the photocatalyst was performed the same procedure as mentioned above in the same processing parameters.

### 2.2.2. Photocatalytic degradation activity test

Tetracycline (TC) was selected to test the photocatalytic degradation performance. In a typical experiment, the photocatalyst (2.5 mg) was added to a tetracycline aqueous solution (5 mL, 10 mg L<sup>-1</sup>), which was saturated with nitrogen gas and sealed with an airtight cap. Then, the suspension was placed in the dark to ensure adsorption-desorption equilibrium. A photocatalytic reactor (400 W metal halide lamp) with a cutoff filter ( $\lambda > 380$  nm) was used as the light source. The system kept on swirling by a magneton during the photocatalytic process. The residual TC concentrations were analyzed by UV-vis spectrophotometer.

### 2.2.3. Dual photocatalytic activity

The photocatalyst (2.5 mg) was dispersed in a saturated TC aqueous solution (5 mL, about 432 mg L<sup>-1</sup>), which was saturated with nitrogen gas and sealed with an airtight cap. Then, the suspension was placed in the dark to ensure adsorption-desorption equilibrium. A photocatalytic reactor (400 W metal halide lamp) with a cutoff filter ( $\lambda > 380$  nm) was used as the light source. The system kept on swirling by a magneton during the photocatalytic process. The produced photoproduct of H<sub>2</sub> was

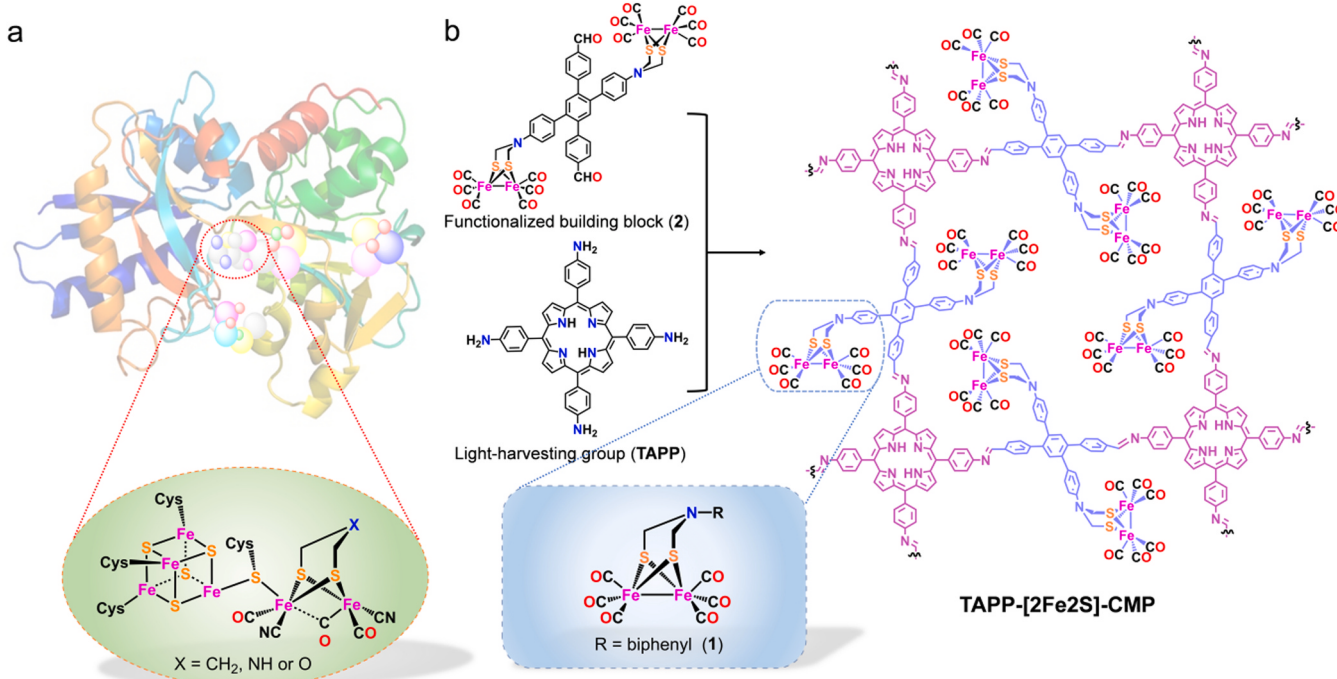


**Fig. 1.** **[a]**, The probable structure of the [FeFe]-hydrogenase active site (being termed as H-cluster). **b**, The strategy for constructing the framework of TAPP-[2Fe2S]-CMP and the structure of its functional sites.

characterized by GC analysis and the residual TC concentrations were analyzed by UV-vis spectrophotometer.

### 3. Results

### *3.1. Synthesis and characterization*

To test the covalent linking strategy, we designed and synthesized two new [FeFe]-hydrogenase model complexes **1** and **2** (Fig. 2a). The successful synthesis of these two compounds was unambiguously characterized by nuclear magnetic resonance (NMR) spectroscopy (Figs. S1–4), Fourier transform infrared (FT-IR) spectroscopy (Fig. 3a) and X-ray crystallography (Fig. 2). The crystallographic-related data of **1** (CCDC: 2150470) and **2** (CCDC: 2150488) were summarized in the Supporting Information.

The [2Fe2S] units in both models **1** (Fig. 2b) and **2** (Fig. 2c) have a pseudo-square-pyramidal geometry, and the corresponding characteristics (Table S1, S2) are also similar to those of azadithiolatodiiron derivatives previously reported [20,21]. Model **2** contains both the main structure of **1** and the aldehyde functional groups, and serves as a building block to construct TAPP-[2Fe2S]-CMP. The [2Fe2S] moieties of **2** bear a structural resemblance to model **1**. By contrast, the dihedral angles around the centric phenyl ring plane in model **2** are slightly different from those in model **1** and precursor compound *p*-TetPB [22].

In order to formulate the “single active-site” effect and improve the

intramolecular electron transport efficiency [23], we designed a conjugated microporous polymer (TAPP-[2Fe2S]-CMP) in which the [2Fe2S] active sites were covalently tethered to the CMP skeleton. The TAPP-[2Fe2S]-CMP was synthesized by Schiff base condensation between model **2** and TAPP at room temperature. Porphyrin, whose tetrapyrrole-derived macrocycle structure widely exists in nature, was selected as the photosensitive group because it has excellent light-harvesting and optoelectronic properties [24]. Additionally, to investigate the effect of covalent tethering of [2Fe2S] clusters to the CMP skeleton, a comparison substance without [2Fe2S] active sites, TAPP-TPDA-CMP, was synthesized by the same synthetic procedure (Figs. S11–13).

The FT-IR spectra of TAPP, **1**, **2** and TAPP-[2Fe2S]-CMP are shown in Fig. 3a. The near-disappearance of primary amine N-H stretching bands (in the vicinity of  $3350\text{ cm}^{-1}$ ) and the attenuation of the aldehydic carbonyl C=O bond at  $1695\text{ cm}^{-1}$  (**2**) in the spectrum of TAPP-[2Fe2S]-CMP indicated the consumption of the reactive groups. Besides, the characteristic stretching bands related to C=N linkages emerged at around  $1624\text{ cm}^{-1}$ , which can be attributed to the formation of imine bonds [25]. The band at about  $962\text{ cm}^{-1}$  related to  $\delta$  N-H in TAPP appeared, which becomes another piece of evidence of the successful formation of the target product [26,27]. Additionally, the TAPP-[2Fe2S]-CMP exhibited the typical peaks of terminal carbonyls (Fe-CO) at about  $2071$ ,  $2033$ , and  $1996\text{ cm}^{-1}$ , which also existed in both building block **2** ( $2073$ ,  $2031$ , and  $1996\text{ cm}^{-1}$ ) and model **1** (in the

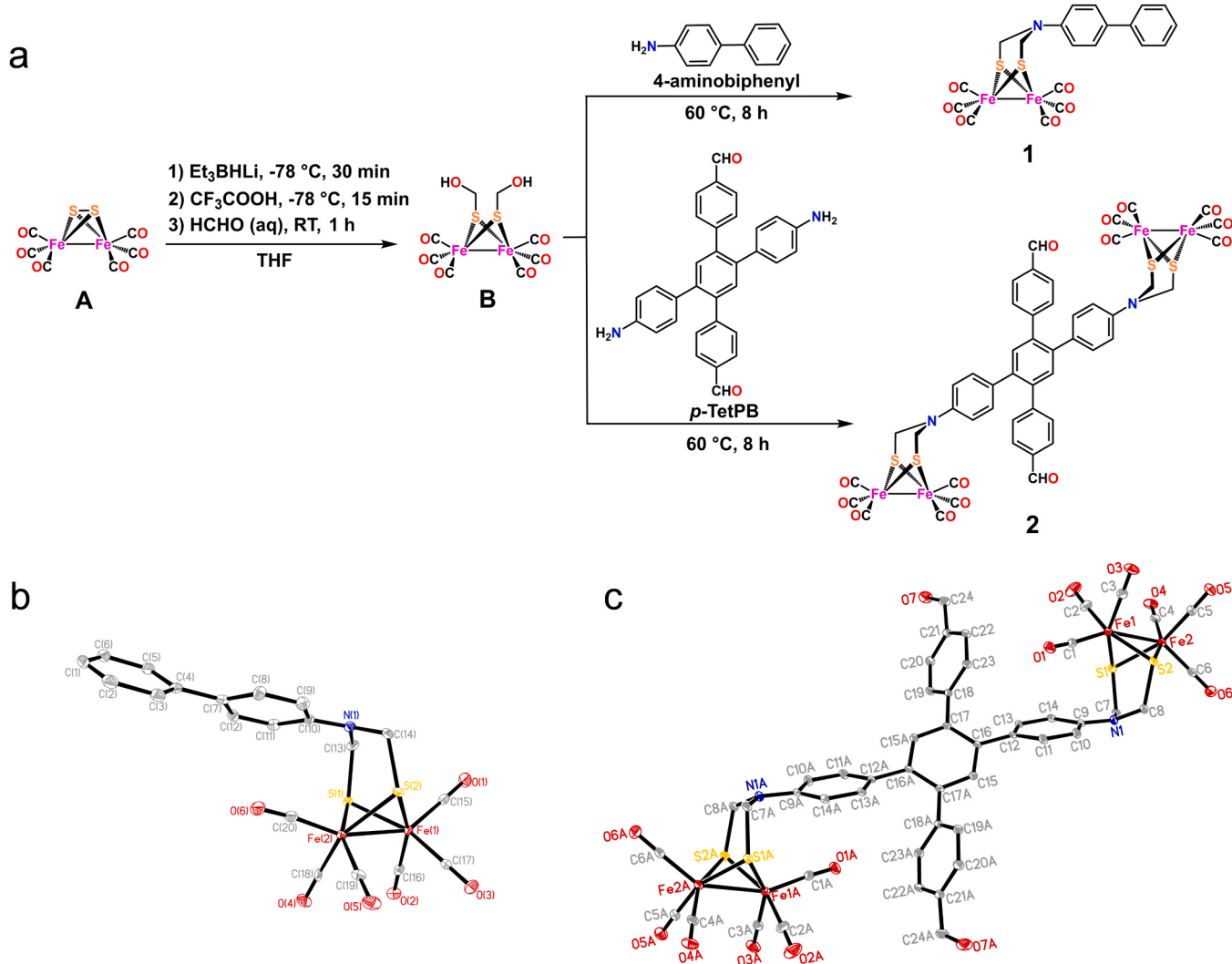


**Fig. 2.** **a**, Synthetic route of model complex **1** and **2**. **b, c**, ORTEP views of **1** and **2**, ellipsoids at 30% probability level.

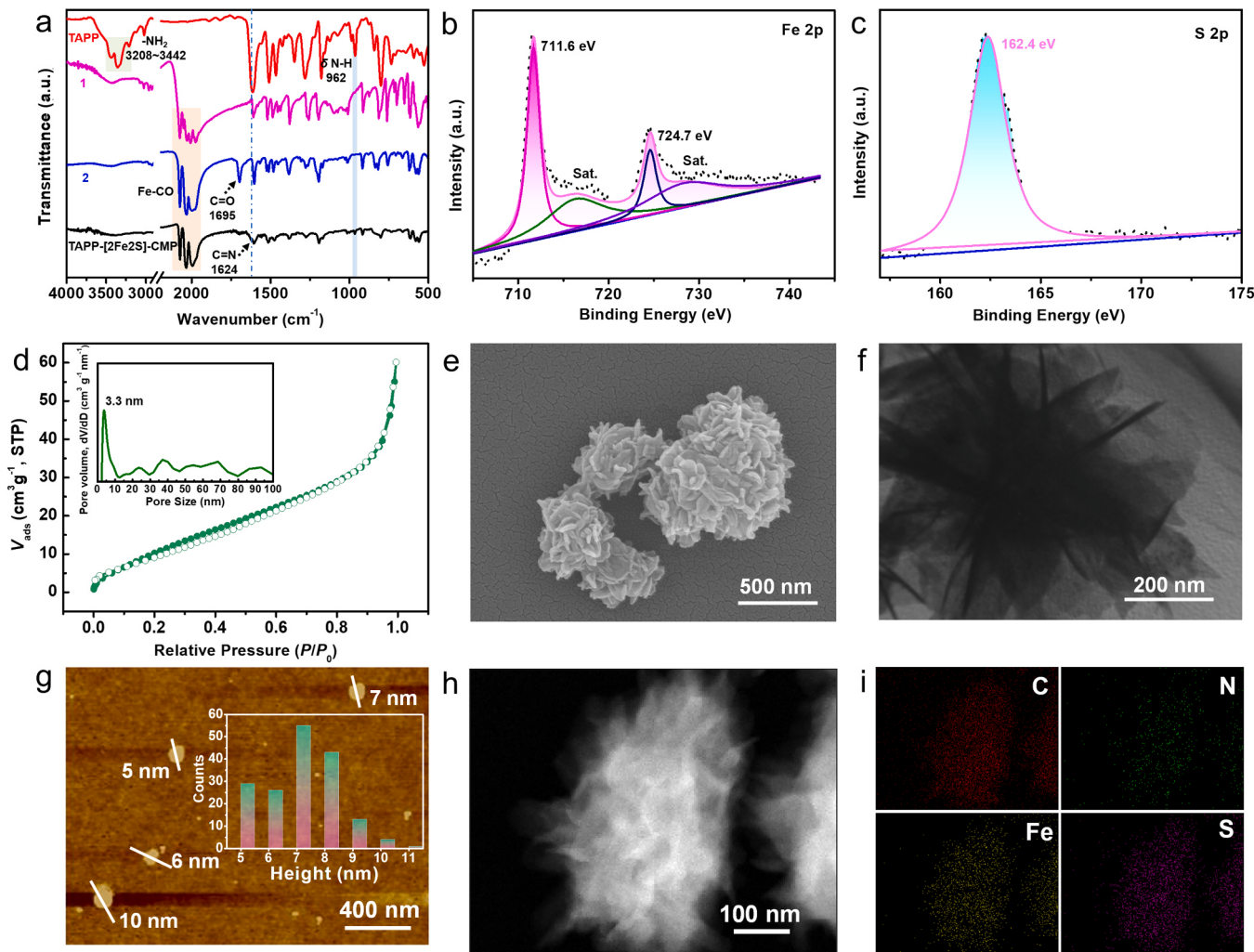


**Fig. 3.** **a**, FT-IR spectra of TAPP, **1**, **2** and TAPP-[2Fe2S]-CMP. **b**, **c**, XPS spectra of TAPP-[2Fe2S]-CMP at the Fe 2p and S 2p energy levels. **d**, Nitrogen adsorption ( $\bullet$ ) and desorption ( $\circ$ ) isotherm profiles of TAPP-[2Fe2S]-CMP at 77 K, (inset) pore size distribution and cumulative pore volume. **e**, **f**, SEM and TEM of TAPP-[2Fe2S]-CMP. **g**, AFM of TAPP-[2Fe2S]-CMP, (inset) thickness distribution of nanosheets. **h**, **i**, High angle annular dark-field scanning transmission electron microscopy (HAADF-STEM) image and elemental mapping of TAPP-[2Fe2S]-CMP.

region of  $2075\text{--}1974\text{ cm}^{-1}$ , suggesting the [2Fe2S] clusters are intact in TAPP-[2Fe2S]-CMP [28,29].

The X-ray photoelectron spectroscopy (XPS) survey of TAPP-[2Fe2S]-CMP showed the presence of the elements of C, N, O, Fe and S (Fig. S5). In the high-resolution XPS spectra, the two main peaks centered at 724.7 and 711.6 eV can be attributed to the  $2p_{1/2}$  and  $2p_{3/2}$  ionizations of the Fe(I) atoms (Fig. 3b), and the peak centered at 162.4 eV is ascribed to the S 2p of the [2Fe2S] clusters (Fig. 3c) [21,30]. All the results above provided further evidence for the successful introduction of [2Fe2S] clusters in the TAPP-[2Fe2S]-CMP.

The powder X-Ray Diffraction (PXRD) of the TAPP-[2Fe2S]-CMP (Fig. S6) presented amorphous characteristics, similar as in other CMP materials [31]. Preliminarily, we speculated that the pseudo-square-pyramidal geometry of the [2Fe2S] clusters reduce the chances of  $\pi\text{-}\pi$  stacking among the building units, which, in turn, may hinder the formation of long-range ordered sheets. Another possible reason could be the relatively mild reaction condition leads to a random displacement of 2D layers and results in an amorphous morphology [32].

In Fig. 3d, the permanent porosity of TAPP-[2Fe2S]-CMP was confirmed by nitrogen sorption analysis at 77 K, giving a Brunauer-Emmett-Teller (BET) value of  $\sim 50\text{ m}^2\cdot\text{g}^{-1}$  with a broad pore size distribution from 1 to 100 nm which indicates hierarchical macro-meso-

microporous texture feature [33]. A prominent distribution peak at 3.3 nm (Fig. 3d, inset) was found, which is similar to the predicted value (3.4 nm) from the theoretical model (Fig. S7).

The scanning electron microscope (SEM) of TAPP-[2Fe2S]-CMP (Fig. 3e) exhibited a loose flower-like microstructure, being with similarity to other reported porphyrin-COF materials [33]. The hierarchical TAPP-[2Fe2S]-CMP superstructure was constructed by several interconnected ultrathin nanosheets with curled edges (Fig. 3f), which were formed probably through a dissolution-reconstruction process. Such an exquisite arrangement could reduce the nanosheet restacking and provide a large surface area, which contributes to exposing more active sites and improving photocatalytic H<sub>2</sub> evolution performance. After being treated by the ultrasonic wave in ethanol for 30 min, hierarchical TAPP-[2Fe2S]-CMP superstructure can be deconstructed into primary nanosheets which exhibit an obvious Tyndall effect in the aqueous solution, ascertaining its nanoscale and high dispersibility (Fig. S8). Atomic Force Microscopy (AFM) characterization (Fig. 3g) proved that the ultrathin nanosheets possess a nanoscale lateral size of less than 200 nm and pretty smooth surfaces with the thickness of 5–10 nm. However, no lattice fringes could be observed in the high-resolution TEM (HRTEM) image of TAPP-[2Fe2S]-CMP (Fig. S9), which is most likely due to its amorphous structure. The elemental mapping images of high-angle annular dark-field scanning transmission electron

microscopy (HAADF-STEM) for TAPP-[2Fe2S]-CMP (Fig. 3h, 3i) exhibited clear evidence for the presence of the element of C, N, Fe and S, and these elements were homogeneously distributed in the TAPP-[2Fe2S]-CMP matrix.

### 3.2. Photocatalytic hydrogen production

Since the structural similarity of the functional moieties in model 1, building block 2 and TAPP-[2Fe2S]-CMP, the redox and catalytic proton reduction properties of the [2Fe2S] active sites were studied using model 1 in the presence of HOAc (0–10 mM) by cyclic voltammetry (CV) technique in CH<sub>3</sub>CN. In the absence of HOAc, a quasi-reversible reduction peak and an irreversible oxidation peak were observed at –1.54 V and +0.50 V, respectively (Fig. 4a). With the addition of HOAc to the CH<sub>3</sub>CN solution of 1, the current intensity of the peak at –1.54 V increased slightly and ceased to grow further with sequential increments of the acid concentration. However, a reduction peak at about –1.80 V emerged and the peak current showed a linear dependence on the concentration of HOAc (Fig. 4a, inset). The above electrochemical behaviors are similar to those of the previous works on the all-carbonyl-substituted diiron azadithiolate model complexes [34,35], indicating the electrocatalytic activity of the [2Fe2S] sites [36].

According to the Ultraviolet-visible (UV/Vis) Diffuse Reflectance spectrometry, TAPP-[2Fe2S]-CMP showed a wide absorption range between 400 and 700 nm (Fig. 4b), offering the possibility of efficient visible light harvesting. The energy gap of TAPP-[2Fe2S]-CMP was determined to be about 1.84 eV according to the Tauc plot obtained from the UV/Vis absorption data (Fig. 4b, inset). As shown in Fig. S10, the positive slopes of the Mott-Schottky plots suggest the n-type semiconductor feature of TAPP-[2Fe2S]-CMP and the flat band position ( $V_{fb}$ ) is about –0.97 V (vs. NHE, pH=7), which can be approximately regarded as the potential of the conduction band (CB) [37]. Combined with the energy gap data above, the valence band (VB) maximum of TAPP-[2Fe2S]-CMP was calculated to be around +0.87 V (vs. NHE, pH=7) [38] (Fig. 5d).

Using TEOA as electron sacrifices, the 5 h photocatalytic H<sub>2</sub> evolution of the TAPP-[2Fe2S]-CMP in an aqueous solution displayed an average rate of 2120 μmol·h<sup>-1</sup>·g<sup>-1</sup> under visible light irradiation (Fig. 4c), which could be comparable to some COF-based visible-light-driven H<sub>2</sub> evolution photocatalytic systems with either non-noble metal (Ni, Co) or even precious metal (Pt) co-catalysts in water or mixed solutions (Table S4). Control experiments showed that no detectable or only traces of H<sub>2</sub> were released without irradiation, TEOA or TAPP-[2Fe2S]-CMP, indicating each factor above is indispensable for the photocatalytic system (Fig. S14). The stability of TAPP-[2Fe2S]-CMP was assessed through FT-IR, SEM, and BET after the photocatalytic test (Fig. S15–17). The H<sub>2</sub> evolution activity of TAPP-[2Fe2S]-CMP remained as much as nearly 81% of the initial value after additional three recycling tests, suggesting adequate recyclability and stability for photocatalytic hydrogen evolution reaction (Fig. 4c, inset).

### 3.3. Dual-function strategy

For economic and environmental concerns, constructing a novel CMP-based dual-function system, in which the costive and sometime even toxic electronic sacrificial reagents were replaced with reductive organic pollutants and H<sub>2</sub> could be generated accompanied by removal of environmentally hazardous residues simultaneously in an aqueous solution, is highly attractive. Tetracycline (TC), a kind of broad-spectrum antibiotic whose residues in aqueous environments may bring about possible risks on public health and ecosystems through drinking water and the food chain, was chosen as a model antibiotic residue in our system.

Firstly, the photodegradation performance of the TAPP-[2Fe2S]-CMP toward TC (10 mg L<sup>-1</sup>) was investigated. As shown in Fig. 4d, TC displayed typical absorption peaks at about 275 and 358 nm, which

were derived from its four six-membered rings arranged linearly with characteristic double bonds [39]. Before the photocatalytic tests, the TAPP-[2Fe2S]-CMP samples underwent 40 min adsorption under dark conditions until reaching a steady state. The photodegradation reactions were triggered under irradiation. It should be pointed out that at the initial stage of the photodegradation test, the absorption intensity at nearly 358 nm decreased slightly faster than that of the peak at about 275 nm, suggesting that the oxidization of the exocyclic unsaturated double bonds or the transformation of the heteroatomic groups, which could lead to the destruction of the original conjugated system in TC, seemed to precede the decomposition of the aromatic nucleus probably [40]. It was demonstrated that the photolysis of TC without a photocatalyst could be ignored according to the blank experiment (Fig. S18), and control experiments towards TC degradation with 1, 2, TAPP, TAPP-TPDA-CMP, TAPP-TPDA-CMP/1, TAPP-TPDA-CMP/2 were shown in Fig. S21.

Based on the absorption intensity at 358 nm, the degradation ratio reached 97% within 120 min, and the degradation behaviors followed the pseudo-first-order kinetics ( $R^2 = 0.98$ ) with an apparent reaction rate constant ( $k$ ) of 0.068 min<sup>-1</sup> within the initial 20 min (Fig. 4e, inset). Moreover, when we analyzed the kinetic characterization of the degradation behaviors during 20–120 min ( $k' = 0.018 \text{ min}^{-1}$ ;  $R^{2'} = 0.95$ ) (Fig. S19), the results were quite different from those of the initial 20 min, which supported the speculation above that the degradation process might be staged or involve some intricate intermediates in our case [41]. The relatively loose flower-like microstructures, ultrathin nanosheets, and hierarchical macro-meso-microporous texture feature of TAPP-[2Fe2S]-CMP would be conducive to enhancing the adsorption affinity toward TC and accelerating the diffusion of TC from bulk to the active sites, which conducted both high absorption ability and degradation efficiency for the photocatalyst [42].

To further elucidate the photocatalytic mechanism, trapping experiments of ·OH, ·O<sub>2</sub><sup>−</sup> and h<sup>+</sup> were conducted by adding different scavengers (0.01 M), which are t-butyl alcohol (TBA), 1,4-benzoquinone (BQ) and ethylenediaminetetraacetic acid (EDTA), respectively [43]. As shown in Fig. 4g, the addition of TBA hardly affected the photocatalytic degradation efficiency of TC, whereas the removal efficiency of TC markedly decreased with the addition of EDTA (from 64% to 41%), suggesting that the h<sup>+</sup> but not the ·OH were the major active species involved in the photocatalytic degradation of TC. Noteworthily, although the solution had been purged by N<sub>2</sub> for 30 min before the photoreaction, the capture experiment showed that ·O<sub>2</sub><sup>−</sup> did participate in the degradation of TC, which hinted that some oxygen might be induced into the system either internally or externally during the irradiation.

To verify the green and sustainable dual-function strategy mentioned above, a series of photocatalytic experiments were carried out in a saturated (about 432 mg·L<sup>-1</sup>) TC solution (pH~5.6) subsequently. As shown in Fig. 4f, with the decrease of TC content, the amount of H<sub>2</sub> emission increased gradually. During five hours, the TAPP-[2Fe2S]-CMP-based system displayed an average photocatalytic H<sub>2</sub> evolution rate of 370 μmol·g<sup>-1</sup>·h<sup>-1</sup> and a concurrent TC removal ratio of about 64%. Compared with the photocatalytic system with TEOA as an electron donor, the efficiency of H<sub>2</sub> releasing in such a dual-function system decreased significantly. The loss of performance may be due to the difference in the initial concentration between TC (~0.97 mmol·L<sup>-1</sup>) and TEOA (~75.4 mmol·L<sup>-1</sup>), or to the interference from side reactions of intermediates during TC decomposition.

### 3.4. Investigation of mechanism

To explore the role of the [2Fe2S] cluster and covalent linkage between the [2Fe2S] cluster and CMP skeleton in the photocatalytic system, corresponding comparative tests were carried out on TAPP-TPDA-CMP and TAPP-TPDA-CMP/1 (physical mixture of TAPP-TPDA-CMP and 1) under the same conditions. As shown in Fig. 4h, without the [2Fe2S] cluster, TAPP-TPDA-CMP exhibited the lowest efficiencies of

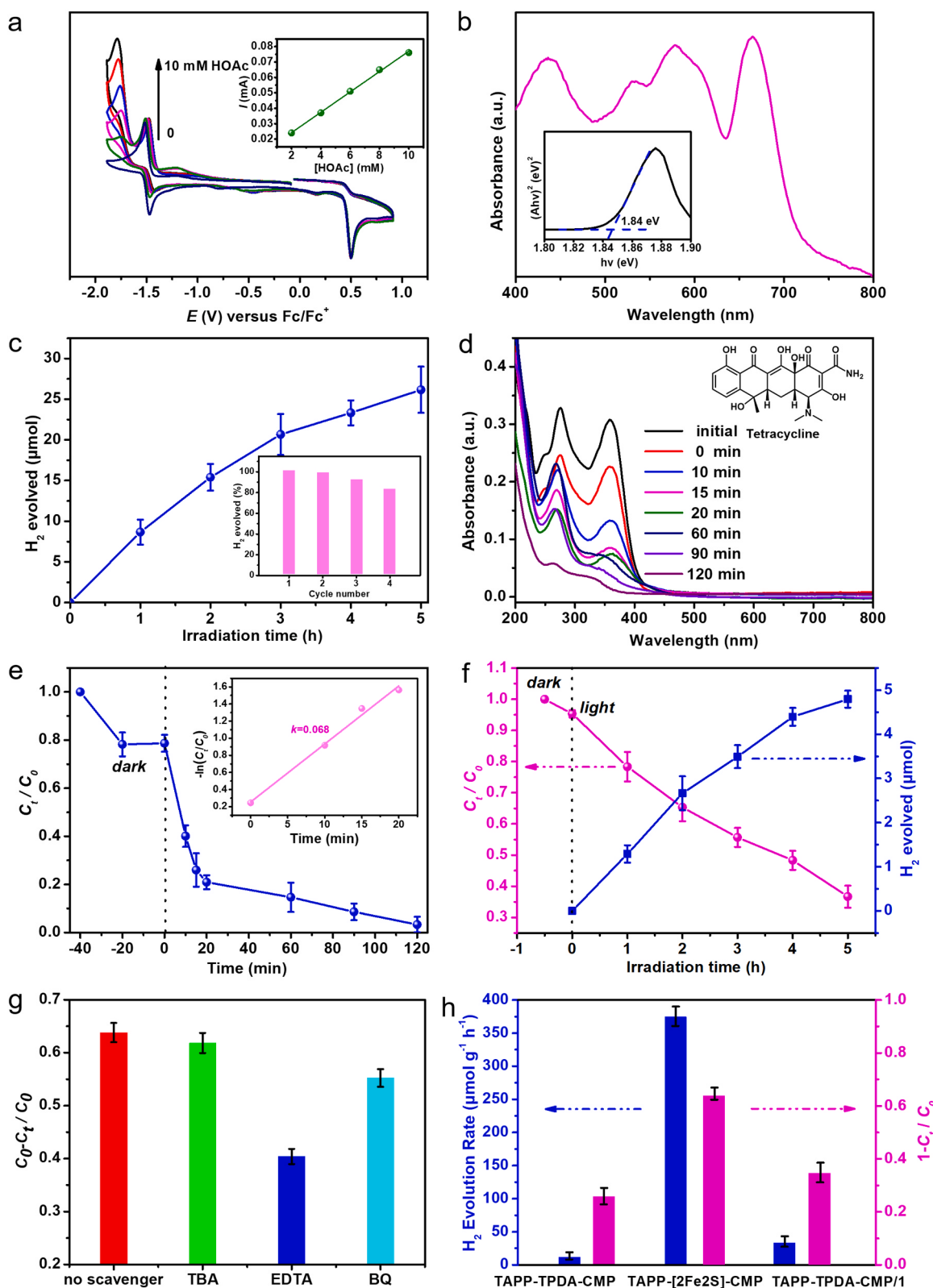


**Fig. 4.** **a**, Cyclic voltammogram of **1** (1 mM) with HOAc (0–10 mM) in 0.1 M of  $n\text{-Bu}_4\text{NPF}_6$  in  $\text{CH}_3\text{CN}$  at a scan rate of  $100 \text{ mV}\cdot\text{s}^{-1}$  and the dependence of the current height of the reduction peak at about  $-1.80 \text{ V}$  on the concentration of HOAc (inset). **b**, UV-vis Diffuse Reflection absorption spectra of TAPP-[2Fe2S]-CMP (Inset: Tauc plot determined from the Kubelka-Munk (K-M) function). **c**, Photocatalytic  $\text{H}_2$  evolution performance of TAPP-[2Fe2S]-CMP under visible light irradiation with TEOA as sacrificial reagent and recyclability of TAPP-[2Fe2S]-CMP (inset). **d**, UV-vis absorption spectra during photodegradation and (inset) the structure of TC. **e**, Photocatalytic degradation curve of TC and (inset) kinetic fitting curve within initial 20 min **f**, Photocatalytic  $\text{H}_2$  evolution performance coupled with degradation of TC. **g**, Trapping experiments. **h**, Results of comparison tests for dual photocatalytic activities.

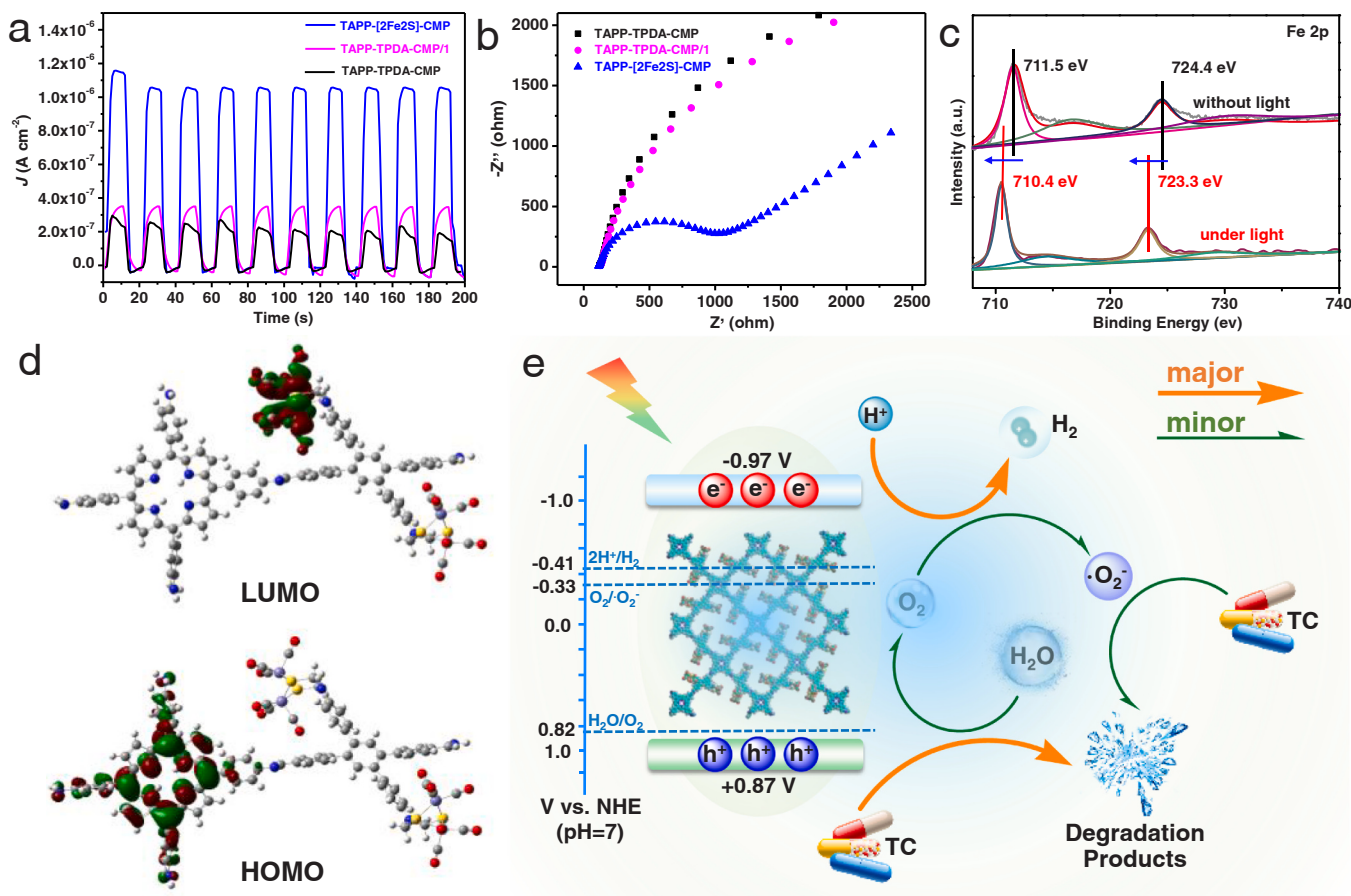


**Fig. 5.** **a**, Transient photocurrent curves and **b**, EIS Nyquist plots of TAPP-[2Fe2S]-CMP, TAPP-TPDA-CMP and TAPP-TPDA-CMP/1 under the visible light irradiation. **c**, High-resolution XPS spectra of Fe 2p for TAPP-[2Fe2S]-CMP without/with light illumination. **d**, Charge density distribution of HOMO and LUMO orbitals for oligomer model of TAPP-[2Fe2S]-CMP. **e**, The plausible mechanism diagram for the dual-functional photocatalytic process of TAPP-[2Fe2S]-CMP.

both  $\text{H}_2$  evolution (negligible) and photodegradation (about 26%). After model **1** was physically mixed with TAPP-TPDA-CMP, the performance of  $\text{H}_2$  generation (trace) and TC removal (nearly 35%) were improved slightly, which was still far behind the system driven by TAPP-[2Fe2S]-CMP.

The results above indicated that 1) porphyrin-based CMP had a good photocatalytic oxidation capacity to photodegrade organic pollutants, which was similar to related materials reported previously [44]; 2) the covalent linkage between the [2Fe2S] cluster and the porphyrin-based CMP skeleton significantly facilitate the separation of excitons and charge transfer, leading to the improvement in both photocatalytic  $\text{H}_2$  evolution and photodegradation of TC.

Transient photocurrent measurements, electrochemical impedance spectroscopy (EIS) [45], and DFT simulations were conducted to further explore the mechanism of covalent linkage of the [2Fe2S] cluster in promoting the exciton separation and the charge transfer. The visible light on/off transient photocurrent curves of TAPP-[2Fe2S]-CMP and its comparison substances were obtained under chopped illumination to explore the charge migration process being responsible for the photocatalytic reaction. In Fig. 5a, the photocurrent density reached approximately triple increments on the TAPP-[2Fe2S]-CMP sample ( $\sim 1.1 \mu\text{A}\cdot\text{cm}^{-2}$ ) in comparison with the TAPP-TPDA-CMP ( $\sim 0.28 \mu\text{A}\cdot\text{cm}^{-2}$ ) and the TAPP-TPDA-CMP/1 ( $\sim 0.36 \mu\text{A}\cdot\text{cm}^{-2}$ ), which manifests the fast photoresponse and indicates the significantly boosted separation and transfer of photoinduced charge carriers [25]. The much smaller semi-circular diameter of TAPP-[2Fe2S]-CMP electrode in the EIS Nyquist plot (Fig. 5b) indicates lower electrical resistance and faster interfacial charge transfer than those of TAPP-TPDA-CMP and TAPP-TPDA-CMP/1. Thus, the covalent linkage between the [2Fe2S] cluster and CMP

skeleton is favorable for electron transfer in the photocatalytic process and boosts the efficiency of photocatalytic  $\text{H}_2$  evolution [46].

Furthermore, both *in situ* XPS measurements and Density functional theory (DFT) calculations were also conducted to understand the photoexcitation process and structure-function relationship. As displayed in Fig. 5c, the high-resolution XPS spectra of Fe 2p shift to lower binding energy direction with light excitation, compared with those of TAPP-[2Fe2S]-CMP without light excitation. These suggest the accumulation of photogenerated electrons on the [2Fe2S] unit in TAPP-[2Fe2S]-CMP with light illumination [47,48]. Besides, combined with the crystal data of model **2**, the DFT calculations shown that the TAPP fragment dominates the HOMO while the LUMO is mainly contributed by the [2Fe2S] part (Fig. 5d). Therein, the charge separation process may readily occur upon light irradiation, which further forms photogenerated electrons located on the accepting [2Fe2S] unit and photogenerated holes centered at the donating TAPP moiety [49]. The spatial separated distribution of frontier orbitals and covalent linkage between TAPP moiety and [2Fe2S] unit enables efficient separation and transfer of photoinduced electrons from the light-harvesting TAPP moiety to the catalytic active [2Fe2S] unit, leading to the superior  $\text{H}_2$  generating performance of TAPP-[2Fe2S]-CMP.

From all the above, a possible mechanism of the dual-functional photocatalytic process was assumed tentatively (Fig. 5e). Under illumination, the photoexcited carriers generated inside the TAPP-[2Fe2S]-CMP skeleton were promoted to separate by the spatial separated frontier orbital alignment, transmitted efficiently through the covalent linkage, and reacted at the active sites on the photocatalyst surface. The photogenerated electrons ( $e^-$ ) might reduce  $\text{H}^+$  (or  $\text{H}_2\text{O}$ ) to produce  $\text{H}_2$ , while the holes ( $h^+$ ) could oxidize the TC adsorbed on the surface of

TAPP-[2Fe2S]-CMP. Meanwhile, some dissolved oxygen (possibly from photocatalytic water splitting) was likely to capture a part of electrons to form superoxide radical ( $\cdot\text{O}_2^-$ ), which may also have a certain effect on the TC photodegradation. Although the hydroxyl radicals ( $\cdot\text{OH}$ ) were also one of the dramatically effective oxidants for decomposing the TC [50], the trapping experiments above showed the effect of  $\cdot\text{OH}$  in our photodegradation TC process could be negligible compared to  $\text{h}^+$  or  $\cdot\text{O}_2^-$ . The probable reaction pathways were described by equations (eq. 1–9) as shown in the Supporting information [38].

#### 4. Discussion

In such a novel porphyrin-based CMP material composed entirely of earth-abundant elements, the covalent link between the light-harvesting moiety and [2Fe2S] site contributes to the high efficient visible-light harvesting, charge separation and transferring. Combined with its hierarchical flower-like microstructures and ultrathin nanosheets, the adsorption affinity toward reagents and the utilization ratio of the active sites were further enhanced. Moreover, the covalently linked skeleton structure of TAPP-[2Fe2S]-CMP not only increases the stability of the framework and accelerates the photoinduced intramolecular electron migration, but also assists in homogeneously immobilizing and dispersing the organometallic [2Fe2S] clusters (only soluble in organic solvent) in the CMP framework, resulting in “single active site” effect [14–16]. This may be conducive to providing water dispersion to inherently hydrophobic [2Fe2S] units and giving full play to the efficiency of the H-cluster mimetics. Thus, the TAPP-[2Fe2S]-CMP exhibited high stability and reusability in photocatalysis, with significant photocatalytic performance.

Undoubtedly, the dual-functional photocatalytic system which can synchronously implement the evolution of eco-friendly clean energy ( $\text{H}_2$ ) and the degradation of environmentally hazardous antibiotic residues (TC) under visible-light irradiation is more conducive to sustainable energy conversion from both economic and environmental perspectives. A possible mechanism for the photocatalytic process was speculated according to the experimental phenomena and theoretical calculation.

We cordially expected that our tentative exploration of the dual-function photocatalytic system based on the covalently linked CMP-“biomimetic catalyst” architecture could offer an avenue to further extend the horizon for the application of non-noble metal photocatalysts, and provide a potentially valuable reference for constructing highly stable photocatalytic systems with effective solar-to-hydrogen efficiencies while abating the pollution to the living ecosystems and additional consumption of scarce resources as far as possible.

#### CRediT authorship contribution statement

**J.Y., S.L., W.H. and G.F.** conceived the idea and designed the experiments. **G.F.** synthesized the materials and conducted most of the characterizations and experiments. **N.S., D.F., W.J., E. Z. and S.Y.** helped with some of the characterizations. **Y.S. and J. Q.** contributed to the DFT calculations. **G.F., J.Y. and S.L.** analyzed the data and wrote the manuscript. All of the authors contributed to writing the paper.

#### Declaration of Competing Interest

The authors declare no competing interests.

#### Data availability

Data will be made available on request.

#### Acknowledgments

This work was financially supported by the National Science

Foundation of China (52073208), the China Postdoctoral Science Foundation (2022M722356) and Seed Foundation of Tianjin University (2023XSU-0020, 2023XQM-0028).

Sincerely appreciate the advice and help from Prof. Yongsheng Liu (at Nankai University) and Kaiyu Jiang (M.S., Nankai University).

This article is also dedicated to commemorating the 100th anniversary of Chemistry at Nankai University (1921–2021) and the 60th anniversary of the Institute of Elemento-organic Chemistry (Nankai University).

#### Appendix A. Supporting information

Supplementary data associated with this article can be found in the online version at doi:10.1016/j.apcatb.2023.123200.

#### References

- [1] H. Nishiyama, T. Yamada, M. Nakabayashi, Y. Maehara, M. Yamaguchi, Y. Kuromiya, Y. Nagatsuma, H. Tokudome, S. Akiyama, T. Watanabe, R. Narushima, S. Okunaka, N. Shibata, T. Takata, T. Hisatomi, K. Domé, Photocatalytic solar hydrogen production from water on a 100-m<sup>2</sup> scale, *Nature* 598 (2021) 304–307, <https://doi.org/10.1038/s41586-021-03907-3>.
- [2] M. Qi, M. Conte, M. Anpo, Z. Tang, Y. Xu, Cooperative coupling of oxidative organic synthesis and hydrogen production over semiconductor-based photocatalysts, *Chem. Rev.* 121 (2021) 13051–13085, <https://doi.org/10.1021/acs.chemrev.1c00197>.
- [3] S. Kampouri, K. Stylianou, Dual-functional photocatalysis for simultaneous hydrogen production and oxidation of organic substances, *ACS Catal.* 9 (2019) 4247–4270, <https://doi.org/10.1021/acscatal.9b00332>.
- [4] W. Wang, J. Chen, C. Li, W. Tian, Achieving solar overall water splitting with hybrid photosystems of photosystem II and artificial photocatalysts, *Nat. Commun.* 5 (2014) 4647, <https://doi.org/10.1038/ncomms5647>.
- [5] C. Zhao, Z. Chen, R. Shi, X. Yang, T. Zhang, Recent advances in conjugated polymers for visible-light-driven water splitting, *Adv. Mater.* 32 (2020), 1907296, <https://doi.org/10.1002/adma.201907296>.
- [6] X. Wang, L. Chen, S. Chong, M. Little, Y. Wu, W. Zhu, R. Clowes, Y. Yan, M. Zwijnenburg, R. Sprick, A. Cooper, Sulfone-containing covalent organic frameworks for photocatalytic hydrogen evolution from water, *Nat. Chem.* 10 (2018) 1180–1189, <https://doi.org/10.1038/s41557-018-0141-5>.
- [7] B. Biswal, H. Vignolo-Gonzalez, T. Banerjee, L. Grunenberg, G. Savasci, K. Gottschling, J. Nuss, C. Ochsnerfeld, B. Lotsch, Sustained solar  $\text{H}_2$  evolution from a thiazolo[5,4-D]thiazole-bridged covalent organic framework and nickel-thiolate cluster in water, *J. Am. Chem. Soc.* 141 (2019) 11082–11092, <https://doi.org/10.1021/jacs.9b03243>.
- [8] J. Wang, J. Zhang, S. Peh, G. Liu, T. Kundu, J. Dong, Y. Ying, Y. Qian, D. Zhao, Cobalt-containing covalent organic frameworks for visible light-driven hydrogen evolution, *Sci. China Chem.* 63 (2020) 192–197, <https://doi.org/10.1007/s11426-019-9658-1>.
- [9] T. Banerjee, F. Haase, G. Savasci, K. Gottschling, C. Ochsnerfeld, B. Lotsch, Single-site photocatalytic  $\text{H}_2$  evolution from covalent organic frameworks with molecular cobaloxime co-catalysts, *J. Am. Chem. Soc.* 139 (2017) 16228–16234, <https://doi.org/10.1021/jacs.7b07489>.
- [10] K. Gottschling, G. Savasci, H. Vignolo-González, S. Schmidt, P. Mauker, T. Banerjee, P. Rovó, C. Ochsnerfeld, B. Lotsch, Rational design of covalent cobaloxime-covalent organic framework hybrids for enhanced photocatalytic hydrogen evolution, *J. Am. Chem. Soc.* 142 (2020) 12146–12156, <https://doi.org/10.1021/jacs.0c02155>.
- [11] B. Kandemir, S. Chakraborty, Y. Guo, K. Bren, Semisynthetic and biomolecular hydrogen evolution catalysts, *Inorg. Chem.* 55 (2016) 467–477, <https://doi.org/10.1021/acs.inorgchem.5b02054>.
- [12] M. Adams, L. Mortenson, J. Chen, Hydrogenase, *Biochim. Et. Biophys. Acta* 594 (1980) 105–176, [https://doi.org/10.1016/0304-4173\(80\)90007-5](https://doi.org/10.1016/0304-4173(80)90007-5).
- [13] H. Wu, X. Li, C. Tung, L. Wu, Bioinspired metal complexes for energy-related photocatalytic small molecule transformation, *Chem. Commun.* 56 (2020) 15496–15512, <https://doi.org/10.1039/D0CC05870J>.
- [14] T. Yu, Y. Zeng, J. Chen, Y. Li, G. Yang, Y. Li, Exceptional dendrimer-based mimics of diiron hydrogenase for the photochemical production of hydrogen, *Angew. Chem. Int. Ed.* 52 (2013) 5631–5635, <https://doi.org/10.1002/anie.201301289>.
- [15] W. Brezinski, M. Karayilan, K. Clary, N. Pavlopoulos, S. Li, L. Fu, K. Matyjaszewski, D. Evans, R. Glass, D. Lichtenberger, J. Pyun, [FeFe]-hydrogenase mimetic metallocopolymers with enhanced catalytic activity for hydrogen production in water, *Angew. Chem. Int. Ed.* 57 (2018) 11898–11902, <https://doi.org/10.1002/anie.201804661>.
- [16] F. Wang, W. Wang, X. Wang, H. Wang, C. Tung, L. Wu, A highly efficient photocatalytic system for hydrogen production by a robust hydrogenase mimic in an aqueous solution, *Angew. Chem. Int. Ed.* 50 (2011) 3193–3197, <https://doi.org/10.1002/anie.201006352>.
- [17] B. Xia, Y. Zhang, B. Shi, J. Ran, K. Davey, S. Qiao, Photocatalysts for hydrogen evolution coupled with production of value-added chemicals, *Small Methods* 4 (2020), 2000063, <https://doi.org/10.1002/smtd.202000063>.

- [18] L. Wang, Z. Zhang, R. Guan, D. Wu, W. Shi, L. Yu, P. Li, W. Wei, Z. Zhao, Z. Sun, Synergistic CO<sub>2</sub> reduction and tetracycline degradation by CuInZnS-Ti<sub>3</sub>C<sub>2</sub>T<sub>x</sub> in one photoredox cycle, *Nano Res.* 15 (2022) 8010–8018, <https://doi.org/10.1007/s12274-022-4661-3>.
- [19] S. Kampouri, T. Nguyen, M. Spodaryk, R. Palgrave, A. Züttel, B. Smit, K. Stylianou, Concurrent photocatalytic hydrogen generation and dye degradation using MIL-125-NH<sub>2</sub> under visible light irradiation, *Adv. Funct. Mater.* 28 (2018), 1806368, <https://doi.org/10.1002/adfm.201806368>.
- [20] J. Hou, X. Peng, J. Liu, Y. Gao, X. Zhao, S. Gao, K. Han, A binuclear isocyanide azadithiolatoiron complex relevant to the active site of Fe-only hydrogenases: synthesis, structure and electrochemical properties, *Eur. J. Inorg. Chem.* (2006) 4679–4686, <https://doi.org/10.1002/ejic.200600452>.
- [21] M. Ahmed, S. Dey, M. Daresbourg, A. Dey, Oxygen-tolerant H<sub>2</sub> production by [FeFe]-H<sub>2</sub>ase active site mimics aided by second sphere proton shuttle, *J. Am. Chem. Soc.* 140 (2018) 12457–12468, <https://doi.org/10.1021/jacs.8b05983>.
- [22] Y. Li, L. Guo, Y. Lv, Z. Zhao, Y. Ma, W. Chen, G. Xing, D. Jiang, L. Chen, Polymorphism of 2D imine covalent organic frameworks, *Angew. Chem. Int. Ed.* 60 (2021) 5363–5369, <https://doi.org/10.1002/anie.202015130>.
- [23] H. Yang, F. Li, S. Zhan, Y. Liu, W. Li, Q. Meng, A. Kravchenko, T. Liu, Y. Yang, Y. Fang, L. Wang, J. Guan, I. Furó, M. Ahlquist, L. Sun, Intramolecular hydroxyl nucleophilic attack pathway by a polymeric water oxidation catalyst with single cobalt sites, *Nat. Catal.* 5 (2022) 414–429, <https://doi.org/10.1038/s41929-022-00783-6>.
- [24] Y. Ding, W. Zhu, Y. Xie, Development of ion chemosensors based on porphyrin analogues, *Chem. Rev.* 117 (2017) 2203–2256, <https://doi.org/10.1021/acs.chemrev.6b00021>.
- [25] W. Chen, L. Wang, D. Mo, F. He, Z. Wen, X. Wu, H. Xu, L. Chen, Modulating benzothiadiazole-based covalent organic frameworks via halogenation for enhanced photocatalytic water splitting, *Angew. Chem. Int. Ed.* 59 (2020) 16902–16909, <https://doi.org/10.1002/anie.202006925>.
- [26] J. Jing, et al., Supramolecular zinc porphyrin photocatalyst with strong reduction ability and robust built-in electric field for highly efficient hydrogen production, *Adv. Energy Mater.* 11 (2021), 2101392.
- [27] J. Jing, J. Yang, Z. Zhang, Y. Zhu, Galactodendriticporphyrinic conjugates as new biomimetic catalysts for oxidation reactions, *Inorg. Chem.* 54 (2015) 4382–4393, <https://doi.org/10.1002/aenm.202101392>.
- [28] L. Song, L. Wang, M. Tang, C. Li, H. Song, Q. Hu, Synthesis, structure, and photoinduced catalysis of [FeFe]-hydrogenase active site models covalently linked to a porphyrin or metalloporphyrin moiety, *Organometallics* 8 (2009) 3834–3841, <https://doi.org/10.1021/om900141x>.
- [29] X. Song, H. Wen, C. Ma, M. Hu, H. Chen, H. Cui, C. Chen, Photocatalytic hydrogen evolution by two comparable [FeFe]-hydrogenase mimics assembled to the surface of ZnS, *Appl. Organomet. Chem.* 28 (2014) 267–273, <https://doi.org/10.1002/aoc.3119>.
- [30] T. Yamashita, P. Hayes, Analysis of XPS spectra of Fe<sup>2+</sup> and Fe<sup>3+</sup> ions in oxide materials, *Appl. Surf. Sci.* 254 (2008) 2441–2449, <https://doi.org/10.1016/j.apsusc.2007.09.063>.
- [31] L. Chen, Y. Yang, D. Jiang, CMPs as scaffolds for constructing porous catalytic frameworks: a built-in heterogeneous catalyst with high activity and selectivity based on nanoporous metalloporphyrin polymers, *J. Am. Chem. Soc.* 132 (2010) 9138–9143, <https://doi.org/10.1021/ja1028556>.
- [32] B. Biswal, S. Chandra, S. Kandambeth, B. Lukose, T. Heine, R. Banerjee, Mechanochemical synthesis of chemically stable isoreticular covalent organic frameworks, *J. Am. Chem. Soc.* 135 (2013) 5328–5331, <https://doi.org/10.1021/ja4017842>.
- [33] X. Hu, J. Jian, Z. Fang, L. Zhong, Z. Yuan, M. Yang, S. Ren, Q. Zhang, X. Chen, D. Yu, Hierarchical assemblies of conjugated ultrathin COF nanosheets for high-sulfur-loading and long-lifespan lithium-sulfur batteries: fully-exposed porphyrin matters, *Energy Stor. Mater.* 22 (2019) 40–47, <https://doi.org/10.1016/j.ensm.2018.12.021>.
- [34] S. Yu, F. Wang, J. Wang, H. Wang, B. Chen, K. Feng, C. Tung, L. Wu, Light-driven hydrogen evolution system with glutamic-acid-modified zinc porphyrin as photosensitizer and [FeFe]-hydrogenase model as catalyst, *Pure Appl. Chem.* 85 (2013) 1405–1413, <https://doi.org/10.1351/PAC-CON-12-08-05>.
- [35] S. Ott, M. Borgström, M. Kritikos, R. Lomoth, J. Bergquist, B. Åkermark, L. Hammarström, L. Sun, Model of the iron hydrogenase active site covalently linked to a ruthenium photosensitizer: synthesis and photophysical properties, *Inorg. Chem.* 43 (2004) 4683–4692, <https://doi.org/10.1021/ic0303385>.
- [36] G. Si, W. Wang, H. Wang, C. Tung, L. Wu, Facile synthesis and functionality-dependent electrochemistry of Fe-only hydrogenase mimics, *Inorg. Chem.* 47 (2008) 8101–8111, <https://doi.org/10.1021/ic800676y>.
- [37] S. Sakthivel, H. Kisch, Daylight photocatalysis by carbon-modified titanium dioxide, *Angew. Chem. Int. Ed.* 42 (2003) 4908–4911, <https://doi.org/10.1002/anie.200351577>.
- [38] J. Zhou, J. Li, L. Kan, L. Zhang, Q. Huang, Y. Yan, Y. Chen, J. Liu, S. Li, Y. Lan, Linking oxidative and reductive clusters to prepare crystalline porous catalysts for photocatalytic CO<sub>2</sub> reduction with H<sub>2</sub>O, *Nat. Commun.* 13 (2022) 4681, <https://doi.org/10.1038/s41467-022-32449-z>.
- [39] X. Ding, S. Mou, Ion chromatographic analysis of tetracyclines using polymeric column and acidic eluent, *J. Chromatogr. A* 897 (2000) 205–214, [https://doi.org/10.1016/S0021-9673\(00\)00779-2](https://doi.org/10.1016/S0021-9673(00)00779-2).
- [40] X. He, T. Kai, P. Ding, Heterojunction photocatalysts for degradation of the tetracycline antibiotic: a review, *Environ. Chem. Lett.* 19 (2021) 4563–4601, <https://doi.org/10.1007/s10311-021-01295-8>.
- [41] X. Li, K. Cui, Z. Guo, T. Yang, Y. Cao, Y. Xiang, H. Chen, M. Xi, Heterogeneous fenton-like degradation of tetracyclines using porous magnetic chitosan microspheres as an efficient catalyst compared with two preparation methods, *Chem. Eng. J.* 379 (2020), 122324, <https://doi.org/10.1016/j.cej.2019.122324>.
- [42] Y. Tang, W. Li, Y. Muhammad, S. Jiang, M. Huang, H. Zhang, Z. Zhao, Z. Zhao, Fabrication of hollow covalent-organic framework microspheres via emulsion-interfacial strategy to enhance lacasse immobilization for tetracycline degradation, *Chem. Eng. J.* 421 (2021), 129743, <https://doi.org/10.1016/j.cej.2021.129743>.
- [43] X. Jiang, L. Wang, F. Yu, Y. Nie, Q. Xing, X. Liu, Y. Pei, J. Zou, W. Dai, Photodegradation of organic pollutants coupled with simultaneous photocatalytic evolution of hydrogen using quantum-dot-modified g-C<sub>3</sub>N<sub>4</sub> catalysts under visible-light irradiation, *ACS Sustain. Chem. Eng.* 6 (2018) 12695–12705, <https://doi.org/10.1021/acssuschemeng.8b01695>.
- [44] Z. Zhang, Y. Zhu, X. Chen, H. Zhang, J. Wang, A full-spectrum metal-free porphyrin supramolecular photocatalyst for dual functions of highly efficient hydrogen and oxygen evolution, *Adv. Mater.* 31 (2019), 1806626, <https://doi.org/10.1002/adma.201806626>.
- [45] C. Li, H. Wu, D. Zhu, T. Zhou, M. Yan, G. Chen, J. Sun, G. Dai, F. Ge, H. Dong, High-efficient charge separation driven directionally by pyridine rings grafted on carbon nitride edge for boosting photocatalytic hydrogen evolution, *Appl. Catal. B* 297 (2021), 120433, <https://doi.org/10.1016/j.apcatb.2021.120433>.
- [46] Y. Zang, R. Wang, P. Shao, X. Feng, S. Wang, S. Zang, T. Mak, Prefabricated covalent organic framework nanosheets with double vacancies: anchoring Cu for highly efficient photocatalytic H<sub>2</sub> evolution, *J. Mater. Chem. A* 8 (2020) 25094–25100, <https://doi.org/10.1039/DOTA10024B>.
- [47] B. Xia, B. He, J. Zhang, L. Li, Y. Zhang, J. Yu, J. Ran, S. Qiao, TiO<sub>2</sub>/FePS<sub>3</sub> S-Scheme heterojunction for greatly raised photocatalytic hydrogen evolution, *Adv. Energy Mater.* 12 (2022) 2201, <https://doi.org/10.1002/aenm.202201449>.
- [48] X. Ruan, C. Huang, H. Cheng, Z. Zhang, Y. Cui, Z. Li, T. Xie, K. Ba, H. Zhang, L. Zhang, X. Zhao, J. Leng, S. Jin, W. Zhang, W. Zheng, S. Ravi, Z. Jiang, X. Cui, J. Yu, A twin S-Scheme artificial photosynthetic system with self-assembled heterojunctions yields superior photocatalytic hydrogen evolution rate, *Adv. Mater.* 35 (2023), 2209141, <https://doi.org/10.1002/adma.202209141>.
- [49] M. Lu, J. Liu, Q. Li, M. Zhang, M. Liu, J. Wang, D. Yuan, Y. Lan, Rational design of crystalline covalent organic frameworks for efficient CO<sub>2</sub> photoreduction with H<sub>2</sub>O, *Angew. Chem. Int. Ed.* 58 (2019) 12392–12397, <https://doi.org/10.1002/anie.201906890>.
- [50] D. Du, W. Shi, L. Wang, J. Zhang, Yolk-shell structured Fe<sub>3</sub>O<sub>4</sub>@Void@TiO<sub>2</sub> as a photo-Fenton-like catalyst for the extremely efficient elimination of tetracycline, *Appl. Catal. B* 200 (2017) 484–492, <https://doi.org/10.1016/j.apcatb.2016.07.043>.